Two-Photon Fluorescence Imaging and Therapy of Cancer Cells with Anisotropic Gold-Nanoparticle-Supported Porous Silicon Nanostructures

Arnaud Chaix, Khalil Rajoua, Vanja Stonajovic, Khaled El cheikh, Elise Bouffard, Anthony Brocéro, Marcel Garcia, Marie Maynadier, Alain Morère, Magali Gary-Bobo, et al.

Two-photon fluorescence imaging and therapy of cancer cells with anisotropic gold nanoparticles supported porous silicon nanostructures

Arnaud Chaix,[a] Khalil Rajoua,[a] Vanja Stonajovic,[b] Khaled El Cheikh,[b] Elise Bouffard,[b] Anthony Brocéro,[b] Marcel Garcia,[b] Marie Maynadier,[c] Alain Morère,[b] Magali Gary-Bobo,[b] Frédéric Favier,[a] Jean-Olivier Durand,[a] and Frédérique Cunin*[a]

Abstract: In this work, we prepared porous silicon (pSi) nanostructures decorated with gold nanoparticles, as probes for cell tissue imaging under two-photon excitation. We also demonstrated that the Au/pSi nanosystems induced cytotoxicity and phototoxicity under two-photon excitation.

Medical imaging is a particular field in medicine where nanotechnologies led to concrete applications with the appearance of commercialized products; a famous example being the use of iron oxide nanoparticles (NP) as contrast agents for MRI (Magnetic Resonance Imaging).[1] Medical imaging is classically used for the diagnosis of disease mainly based on the visualization of the organ anatomy, in complement with biological and clinical tests. It is also an essential tool for clinical research and new drug discovery.

In particular, molecular imaging which uses probes to visualize tissues and cells functions, aims to understand the molecular biology of the disease and evaluate its extent in order to guide therapy towards a personalized medicine. Moreover it also aims to identify disease in its earliest stage, without the use of invasive surgery or biopsy.[2] Molecular imaging mainly uses technologies of magnetic resonance imaging, nuclear medicine (positron emission tomography), optical imaging and ultrasons.[3] Optical imaging with the development of non-linear optics approaches has allowed major advances in tissue imaging and biomedical research.[4] In particular two-photon fluorescence microscopy by operating with excitation light in the near-infrared (NIR) spectral window (700-1350nm), where biomolecules are less absorbing and scattering, allows light tissue penetration at depth non accessible to conventional confocal microscopy. In addition, by concentrating the excitation light at the focus area, two-photon fluorescence microscopy also allows 3-D spatial resolution reducing photodamage to surrounding living tissues. Nanoparticles of noble metal in particular gold NP display unique optical properties such as surface plasmon resonance. They also display non-linear optical properties. Gold NP display strong two-photon photoluminescence and were shown to act as excellent two-photon imaging contrast agents.[5] In addition, highly enhanced optical responses can be obtained by modulating their size and shape.[6] For example, anisotropic gold nanostructures such a gold nanorods can display two-photon cross section absorption (TPACS) in the range of that of quantum dots, much higher than organic fluorophores, while not displaying the heavy-metal inherent toxicity of the quantum dots.

In this work, gold nanoparticles (AuNPs) of 12 nm, a quite low diameter for long-term circulation in blood, were adsorbed onto the surface of mesoporous silicon nanoparticles (pSiNPs) of about 200 nm, for their vectorization and for cell targeting purpose. With their high surface area, pSiNPs are great vector systems, easily functionalizable with organic ligands by mean of simple surface chemistry, and fully biodegradable *in vivo*.[7] In addition, pSiNPs can be excited by near infrared (NIR) two-photon excitation light. Here the pSiNPs also carried targeting agent mannose to enable endocytosis of the pSi nanocarriers.[7b, 8] The AuNPs were observed to preferentially self-assemble in anisotropic nanostructures or nanochaplets assimilable to nanorods onto the pSiNPs surface. The potential of the system for two-photon cell imaging and photodynamic therapy (PDT) was studied. In addition, the synergic cytotoxic effect of AuNPs immobilized onto the pSiNPs was analysed. pSiNP were prepared by electrochemical route and prolonged ultrasonic treatment, following procedures previously established in our group and detailed in the supporting information part.[7b, 8a, 9] Transmission

[a] Dr A. Chaix, Dr K. Rajoua, Dr. F. Favier, Dr. J.-O. Durand, Dr F. Cunin
Institut Charles Gerhardt Montpellier
UMR5253CNRS-ENSCM-UM
Place Eugene Bataillon, CC 1701, 34095 Montpellier cedex 5, France
E-mail : Frederique.cunin@enscm.fr

[b] Dr V. Stonajovic, Dr K. El Cheikh, Dr. E. Bouffard, A. Brocero, Dr. M. Garcia, Dr A. Morere, Dr. M. Gary-Bobo
Institut des Biomolécules Max Mousseron
UMR5247CNRS-UM
15 Avenue Charles Flahault, BP 14491, 34093 Montpellier Cedex 05, France.

[c] Dr M. Maynadier
NanoMedSyn
15 Avenue Charles Flahault 34093 Montpellier Cedex, France

Supporting information for this article is given via a link at the end of the document.

Electron Microscopy (TEM) showed mesoporous nanoparticles of heterogeneous shape with oriented pore channels (**Fig. 1A**).

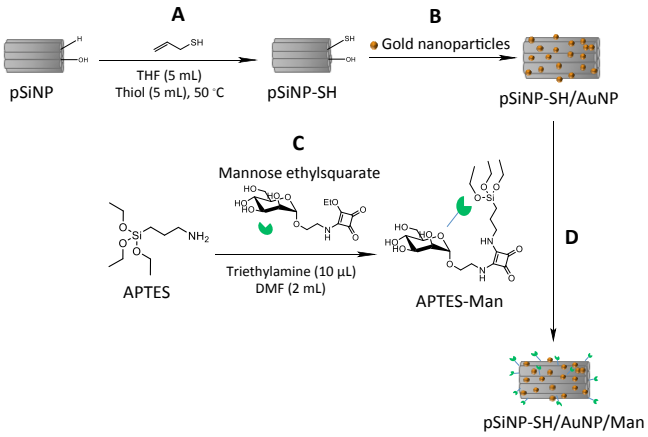

Scheme 1. Reaction pathways for (A) the hydrosilylation of allyl mercaptan with pSiNPs, (B) the complexation of AuNPs on thiolated pSiNPs, (C) the coupling of mannose ethyl squarate with aminopropyltriethoxysilane, (D) the grafting of mannose ethyl squarate onto the pSiNPs by silanization.

The hydrodynamic diameter of the pSiNPs, measured by Dynamic Light Scattering (DLS), was centered at 169 nm with a polydispersity of 0.2, and was consistent with the observations from the TEM images (**Fig. S1, ESI**). Nitrogen adsorption/desorption analysis confirmed the mesoporous texture of the pSiNPs with an average pore diameter of 19.5 nm and a high specific surface area of 461 m²/g (**Fig. S2, a, ESI**). Furthermore, X-ray diffraction pattern indicated the presence of a crystalline structure (**Fig. S2, b, ESI**), in line with the textural and structural features expected for pSiNPs.[7b] In this work, AuNPs were prepared according to the Frens-Turkevich method.[10] The gold NPs exhibited a spherical shape with a 12 ± 1 nm diameter (**Fig. S3, ESI**). In addition, a characteristic plasmon band for Au was observed at 522 nm by UV-vis spectroscopy (**Fig. S4, ESI**). AuNPs were adsorbed onto the surface of the pSiNPs previously hydrosilylated with allyl mercaptan, by complexation with the thiol functions **(Scheme 1. A-B)**.

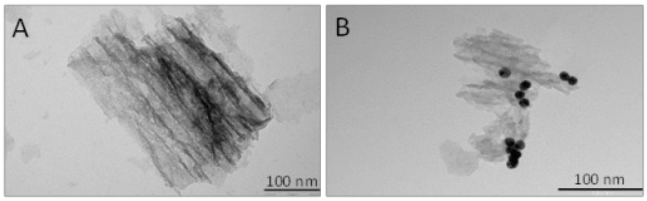

Figure 1. TEM images of pSiNP (A) pSiNP-SH/AuNP (B).

In addition, targeting agent mannose, modified with aminopropyltriethoxysilane (APTES) was covalently attached to the pSiNP-SH/AuNP surface by silanization **(Scheme 1. C-D)**. The mannose was functionalized at its anomeric position with an ethylsquarate spacer arm available for selective covalent reaction with the APTES. The mannose ethylsquarate was prepared according to procedures described in the ESI part. Here the bare pSiNPs exhibited both silicon hydride (Si-H) on their surface co-existing with silicon hydroxide (Si-OH) formed by natural post-oxidation of the Si-H after sample preparation, without any additional oxidative treatment. This allowed chemical functionalization of the pSiNPs by mean of both hydrosilylation and silanization chemistries.

The successful functionalization of the pSiNPs with allyl mercaptan and with mannose ethyl squarate was confirmed by Diffuse Reflectance Infrared Fourier Transform (DRIFT) spectroscopy (**Fig. S5, ESI**). The amount of grafted mannose was determined spectrophotometrically by reaction with resorcinol. A loading of 42 µg of mannose ethylsquarate per mg of pSiNP was obtained. (**Fig. S6, ESI**).

The complexation of the AuNPs with the S-H group from the allyl mercaptan was evidenced by Transmission Electron Microscopy (TEM) as shown on **fig. 1B**. The AuNPs were observed to form anisotropic aggregates or nanochaplets at the surface of the pSiNPs rather than adsorb in the porous structure in a monodisperse manner. Tomography images presented in **Fig. S6** also indicated the immobilization of AuNP aggregates at the surface of the pSiNPs. The wide-angle powder X-Ray Diffraction (XRD) patterns clearly evidenced the presence of the AuNP on pSiNP as well (**Fig. S8, ESI**), with a peak at 38° corresponding to the Au (111) crystallographic planes, absent in the bare pSiNP XRD patterns (**Fig. S2, b, ESI**). The Au plasmon band at 522 nm was observed for pSiNP-SH/AuNP, while no absorption band in the range of 400-600 nm was noticed in the pSiNPs UV-vis absorbance spectrum (**Fig. S4, ESI**). In addition, measurements of the hydrodynamic diameter of the formulations nanoparticles by DLS, shown an increase in diameter of about 58 nm after complexation of the AuNPs onto the pSiNPs. This is an additional indication of the formation of AuNP aggregates at the external surface of the pSiNPs. After grafting of mannose, average hydrodynamic diameter of 328 nm was recorded for the nanoparticles (**Fig.**

S1, ESI) suggesting efficient surface chemical modification of the pSiNP with mannose. The mass loading of Au in pSiNP-SH/AuNP, determined by energy dispersive X-Ray spectrometry (EDX), was 19% in weight (**Fig. S9, ESI**). Finally, Scanning Electron Microscopy (SEM) images in the retrodiffused and secondary electron modes pointed out an homogeneous distribution of gold nanoaggregates and nanochaplets on the surface of the pSiNPs (**Fig. S10, ESI**).

The potential of the nanosystems for two-photon fluorescence imaging was investigated. The pSiNP, the pSiNP-SH/AuNP and the pSiNP-SH/AuNP/Man formulations were incubated with human MCF-7 breast cancer cells for 5 h. The confocal microscopy experiment was realized on living cells by mean of a LSM 780 Carl Zeiss confocal microscope. The membranes of the cells were stained with a membrane marker (cell mask) and visualized at 560 nm. The two-photon imaging was performed with the Chameleon laser of LSM 780 (Laser input 3 W) at a low power (5% of the laser input) under 800 nm excitation wavelength. The fluorescence imaging experiments presented in **Fig. 2** show no detectable fluorescence with pSiNPs. Here, it is likely that bare pSiNPs neither internalized cells efficiently nor strongly absorbed the 800 nm two-photon excitation (TPE) light.[7b] In contrast, strong blue color from AuNP aggregates was observed for pSiNP-SH/AuNP and for pSiNP-SH/AuNP/Man incubated with cells, under 800 nm TPE. The pSiNP-SH/AuNP and pSiNP-SH/AuNP/Man appeared to be localized mostly inside the cells thus demonstrating the successful cellular internalization of the nanosystems, and also confirming the important potential of AuNPs for two-photon fluorescence imaging.[5] Furthermore, more efficient cell internalization was obtained when the nanoparticles were functionalized with targeting agent mannose, as more blue luminescent aggregates were observed for pSiNP-SH/AuNP/Man compared to pSiNP-SH/AuNP. This results previously observed in our group for other systems confirmed the role that mannose moiety play in cellular internalization of pSiNPs.[7b, 8a, 8b, 11]

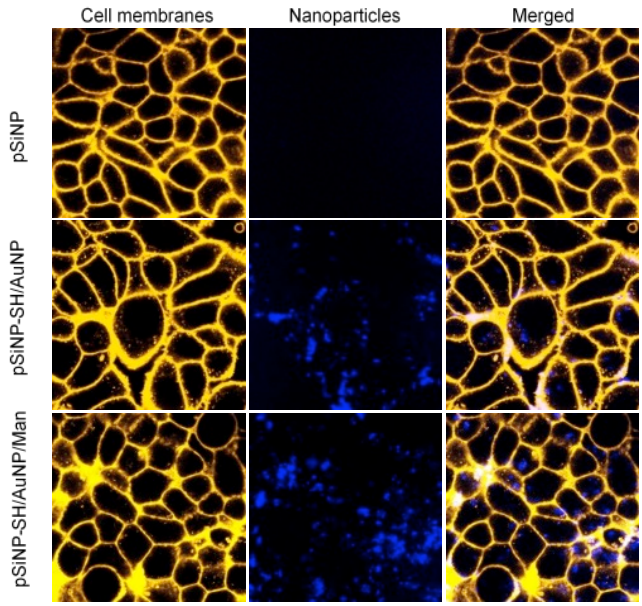

Figure 2. Two-photon fluorescence imaging of MCF-7 breast cancer cells. MCF-7 cells were incubated 5 h with 80 µg.mL^{-1} nanoparticles (pSiNP, pSiNP-SH/AuNP and pSiNP-SH/AuNP/Man).

The photodynamic effect of the nanoparticle systems under TPE was then investigated *in vitro* on MCF-7 breast cancer cells. MCF-7 cells were incubated for 5 h with pSiNP, pSiNP-SH/AuNP and pSiNP-SH/AuNP/Man at 80 µg.mL^{-1}. Cells were exposed to three TPE irradiation at 800 nm. The TPE for PDT was performed at a maximum laser power (input power of 3 W at 800 nm), the well was irradiated with three scans of 1.57 s each in four different areas without overlaps between irradiated areas with the smallest objective (Carl Zeiss 10-fold magnification/objective 0.3 EC Plan-Neofluar). Two days after irradiation, the percentage of living cells was determined by MTT assay **(Fig. 3 A)**. Importantly, with 100% of cell survival for pSiNP and 84% and 80% of cell survival for pSiNP-SH/AuNP and pSiNP-SH/AuNP/Man respectively, the formulations were found to be non toxic or poorly toxic in the absence of irradiation; in addition, no damage to the cells was caused by TPE irradiation itself. **(Fig. 3 A-B)**. Under TPE, the pSiNP induced 15% cells death confirming the capacity of porous silicon to produce cytotoxic reactive oxygen species (ROS) upon 2-photon irradiation.[7b] When carrying AuNPs, toxicity of the pSiNP-based nanosystems substantially increased with 40% of cell death for pSiNP-SH/AuNP. When mannose was present, up to 50% of cell death was achieved for pSiNP-SH/AuNP/Man as mannose moiety enhanced the cellular internalization of the nanoparticles (**Fig. 3 A**). Here the toxicity observed for the nanosystems came from pSiNP and AuNP phototoxicity under TPE, combined with intrinsic AuNP cytotoxicity. To confirm the nature of the toxic entities produced by the NP systems under TPE and the formation of ROS, a DCFDA assay was performed on

MCF-7 cancer cells before and after a TPE at 800 nm. Cells were incubated for 5 hours at a concentration of 80 µg.mL^{-1} with pSiNP, pSiNP-SH/AuNP and pSiNP-SH/AuNP/Man, and then exposed to DCFDA for 45 minutes. Cells were rinsed and imaged before and after laser irradiation. Oxidative stress was measured in MCF-7 cells with the DCFDA that fluoresces when exposed to intracellular peroxides. A marginal level of fluorescence was detected when control cells were stained with DCFDA. Control cells showed very low fluorescence levels when stained with DCFDA compared to nanoparticles treated cells. A clear ROS production was observed with pSiNP, pSiNP-SH/AuNP and pSiNP-SH/AuNP/Man nanoparticles after TPE at 800 nm (**Fig. 3 C**). Finally no ROS production was detected in the absence of irradiation, which confirms that the pSiNP-SH/AuNP based systems specifically induce oxidative stress generation in MCF-7 cells under TPE exposure.

In summary, porous silicon nanovectors carrying gold nanoparticles and functionalized with mannose moieties as tumor targeting agents were successfully designed, and demonstrated remarkable capability as 2-photon imaging contrast-agent. Important photodynamic efficiency of the nanovectors was also observed in human breast cancer cells, with the formation of reactive oxygen species when exposed to two-photon light excitation. Such targeted pSi/Au nanovectors provide an interesting new opportunity for 2-photon imaging and PDT, and an interesting potential for further clinical research and theranostic applications.

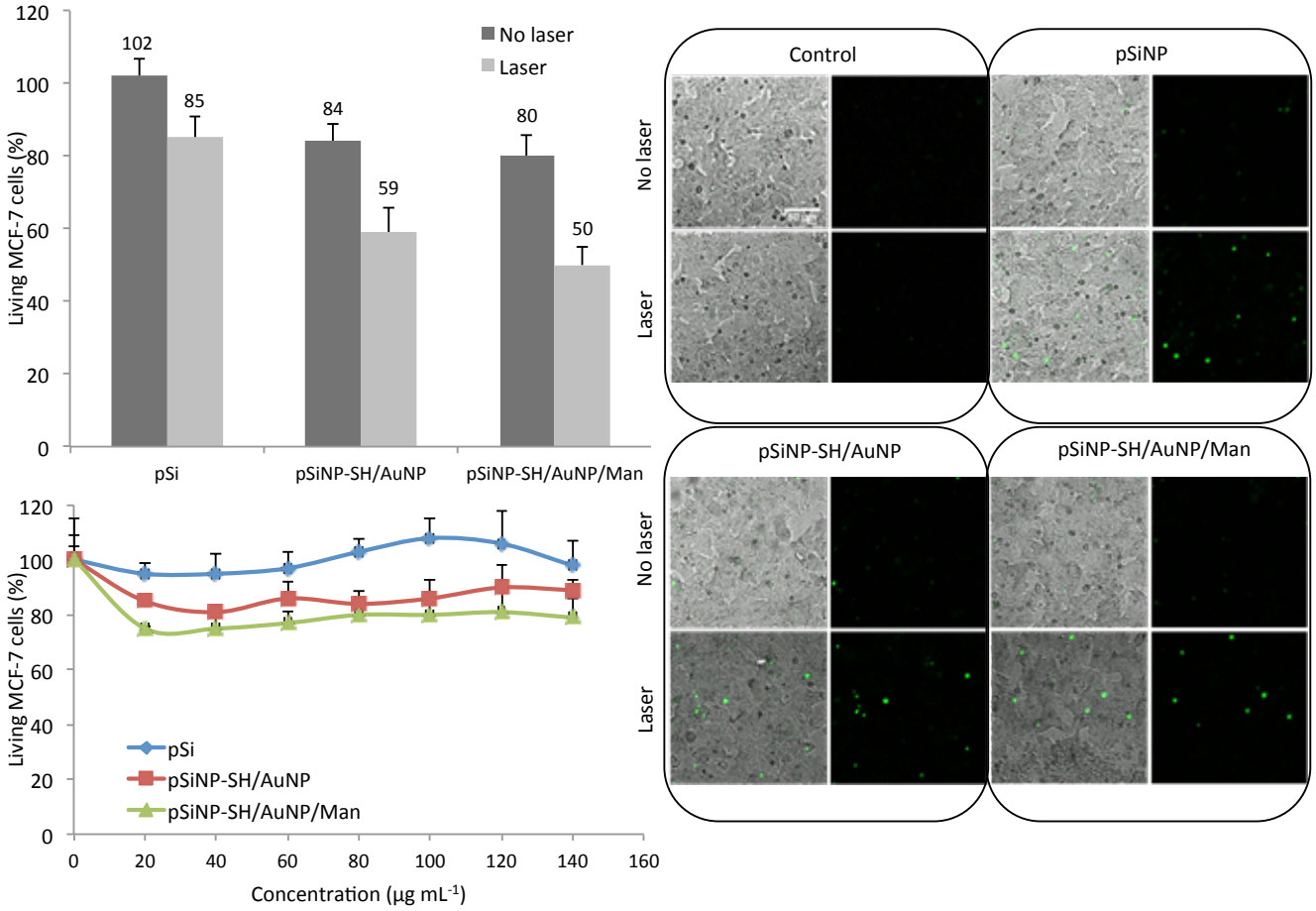

Figure 3. Phototoxicity and cytotoxicity of pSiNP, pSiNP-SH/AuNP and pSiNP-SH/AuNP/Man. (A) In vitro photodynamic effect of nanoparticles on MCF-7 cells. The cells were incubated 5 h with 80 µg.mL^{-1} nanoparticles. Bar graphs represent means of triplicates ± standard deviations. (B) Cytotoxicity study of increasing concentrations of nanoparticles incubated 72 h with MCF-7 cells and submitted to cell death quantification (MTT assay). (C) Detection of intracellular ROS by DCFDA assay in MCF-7 cancer cells.

Experimental Section

Preparation of porous silicon nanoparticles pSiNP

Boron-doped p^{++}-type Si (0.8-1.2 mΩ.cm resistivity, <100> orientation) from Siltronix (France) was electrochemically etched in a 3:1 (v:v) solution of aqueous 48% hydrofluoric acid (HF):absolute ethanol (Sigma-Aldrich). Etching was performed in a Teflon cell with a platinum ring counter electrode. A constant current of 167 mA.cm^{-2} was applied for 150

s, and then the sample was rinsed 3 times with ethanol. The porous layer was then removed from the substrate by application of a constant current of 4 $mA.cm^{-2}$ for 250 s in an electrolyte solution containing 1:20 (v:v) aqueous 48% hydrofluoric acid:absolute ethanol. After 3 rinses with ethanol, the porous layer was placed in ethanol in a glass vial. After degassing the sample for 20 min under a nitrogen stream, the porous silicon film was fractured by ultrasonication during 16 h. The largest particles were then removed by spinning them down by centrifugation at 3,000 rpm for 2 min (Minispin, Eppendorf). In order to remove the smallest particles, the solution was finally centrifuged at 14,000 rpm for 30 min (centrifuge Eppendorf 5804). The pellet was then redispersed in absolute ethanol.

Preparation of gold nanoparticles AuNP

*A*ll glassware used in the following procedures was cleaned using freshly prepared “aqua regia” solution (3:1 $HCl:HNO_3$) and rinsed thoroughly with H_2O prior to use. All solutions were prepared with distilled water (Elga H_2O purification system, $\sigma \geq 18.2\ M\Omega.cm^{-1}$). Gold nanoparticles were prepared by the Turkevich-Frens's method.[10] Briefly, 5 mL of a sodium citrate tribasic dihydrate, $C_6H_5Na_3O_7,2H_2O$, (Sigma-Aldrich) 38.8 $mmol.L^{-1}$ aqueous solution was added to a 50 mL boiling aqueous 1.0 $mmol.L^{-1}$ solution of sodium tetrachloroaurate (III) dihydrate, $NaAuCl_4,2H_2O$ (99.99%, Alfa Aesar) under vigorous stirring. During the 20 min stirring, the colour of the solution gradually turned from yellow to dark blue and to red at the end. Then, the solution was gradually cooled down to room temperature and the stirring was extended by 20 min. Particle sizes diameter were determinate by analysis of transmission electron microscopy (TEM) photographs and the average particle diameters were observed in the range of 11-13 nm.

Acknowledgements

The ANR (Agence Nationale pour la recherche, programme Blanc inter I SIMI 10, edition 2012) and Institut Carnot Chimie Balard are gratefully acknowledged. The authors thank T. Cacciaguerra and Jonas Croissant for the TEM and SEM imaging respectively. M Gary-Bobo is grateful to the Région Languedoc-Roussillon (Research Grant “Chercheur(se)s d’Avenir – Editions 2013, 2013-098085).

Conflicts of interest

There are no conflicts of interest to declare.

Keywords: porous silicon nanoparticles • gold nanoparticles • two-photon imaging • photodynamic therapy • targeting agent

[1] S. Laurent, D. Forge, M. Port, A. Roch, C. Robic, L. V. Elst, R. N. Muller, *Chem Rev* **2008**, *108*, 2064-2110.
[2] a) A. R. Pantel, D. A. Mankoff, *Cancer Lett* **2017**, *387*, 25-31; b) D. A. Mankoff, M. D. Farwell, A. S. Clark, D. A. Pryma, *Jama Oncol* **2017**, *3*, 695-701.
[3] D. A. Mankoff, *J Nucl Med* **2007**, *48*, 18n-+.
[4] P. Dufour, S. Dufour, A. Castonguay, N. McCarthy, Y. De Koninck, *M S-Med Sci* **2006**, *22*, 837-844.
[5] a) T. D. Rane, A. M. Armani, *Plos One* **2016**, *11*; b) N. Y. Gao, Y. Chen, L. Li, Z. P. Guan, T. T. Zhao, N. Zhou, P. Y. Yuan, S. Q. Yao, Q. H. Xu, *J Phys Chem C* **2014**, *118*, 13904-13911.
[6] S. Eustis, M. A. El-Sayed, *Chem Soc Rev* **2006**, *35*, 209-217.
[7] a) J. H. Park, L. Gu, G. von Maltzahn, E. Ruoslahti, S. N. Bhatia, M. J. Sailor, *Nat Mater* **2009**, *8*, 331-336; b) E. Secret, M. Maynadier, A. Gallud, A. Chaix, E. Bouffard, M. Gary-Bobo, N. Marcotte, O. Mongin, K. El Cheikh, V. Hugues, M. Auffan, C. Frochot, A. Morere, P. Maillard, M. Blanchard-Desce, M. J. Sailor, M. Garcia, J. O. Durand, F. Cunin, *Adv Mater* **2014**, *26*, 7643-7648.
[8] a) A. Chaix, K. El Cheikh, E. Bouffard, M. Maynadier, D. Aggad, V. Stojanovic, N. Knezevic, M. Garcia, P. Maillard, A. Morere, M. Gary-Bobo, L. Raehm, S. Richeter, J. O. Durand, F. Cunin, *J Mater Chem B* **2016**, *4*, 3639-3642; b) W. Liu, A. Chaix, M. Gary-Bobo, B. Angeletti, A. Masion, A. Da Silva, M. Daurat, L. Lichon, M. Garcia, A. Morere, K. El Cheikh, J. O. Durand, F. Cunin, M. Auffan, *Nanomaterials (Basel)* **2017**, *7*; c) M. Gary-Bobo, Y. Mir, C. Rouxel, D. Brevet, I. Basile, M. Maynadier, O. Vaillant, O. Mongin, M. Blanchard-Desce, A. Morere, M. Garcia, J. O. Durand, L. Raehm, *Angew Chem Int Ed Engl* **2011**, *50*, 11425-11429.
[9] N. Z. Knezevic, V. Stojanovic, A. Chaix, E. Bouffard, K. El Cheikh, A. Morere, M. Maynadier, G. Lemercier, M. Garcia, M. Gary-Bobo, J. O. Durand, F. Cunin, *J Mater Chem B* **2016**, *4*, 1337-1342.
[10] J. Turkevich, P. C. Stevenson, J. Hillier, *Discuss Faraday Soc* **1951**, 55-&.
[11] M. Gary-Bobo, Y. Mir, C. Rouxel, D. Brevet, I. Basile, M. Maynadier, O. Vaillant, O. Mongin, M. Blanchard-Desce, A. Morere, M. Garcia, J. O. Durand, L. Raehm, *Angew Chem Int Edit* **2011**, *50*, 11425-11429.